

# Enhanced and tunable electric dipole-dipole interactions near a planar metal film

Lei-Ming Zhou,<sup>1,2</sup> Pei-Jun Yao,<sup>3,\*</sup> Nan Zhao,<sup>2</sup> and Fang-Wen Sun<sup>1,†</sup>

<sup>1</sup>Key Laboratory of Quantum Information, University of Science and Technology of China, Hefei 230026, China

<sup>2</sup>Beijing Computational Science Research Center, Beijing 100193, China

<sup>3</sup>University of Science and Technology of China, Hefei 230026, China

(Dated: July 12, 2017)

We investigate the enhanced electric dipole-dipole interaction by surface plasmon polaritons (SPPs) supported by the planar metal film waveguide. By taking two nitrogen-vacancy (NV) center electric-dipoles in diamond as an example, both the coupling strength and collective relaxation of two dipoles are studied with numerical Green Function method. Compared to the two-dipole coupling on planar surface, metal film provides stronger and tunable coupling coefficients. Enhancement of the interaction between coupled NV center dipoles could have applications in both quantum information and energy transfer investigation. Our investigation provides a systematical result for experimental applications based on dipole-dipole interaction mediated with SPPs on planar metal film.

## I. INTRODUCTION

Interaction between photon and atom is one of the most important topics in modern physics and applications. Mediated by photons, individual atoms can interact with each other, which has been a kernel in fundamental physics, ranging from super-radiance [1–3] to quantum entanglement [4]. Investigation on interacting atoms or molecules is also essential for the understanding of energy relaxation and high-efficiency energy transfer [5–8] in chemical and biological processes [9–11]. In addition to natural atoms and molecules, artificial atoms [12, 13] with excellent tailorability and controllability could provide opportunities for studying the light-matter interaction and for developing devices with novel functions. Among these artificial atoms, nitrogen vacancy (NV) center in diamond is a very typical example. NV centers can be generated in diamond crystal with controllable distance [14]. Accompanying with outstanding features, such as long decoherence time, stable photon emission, and mature characterization and manipulation techniques by microwave and laser [15, 16], NV centers can be well applied in quantum information techniques and biology sensing. Moreover, with the recently developed super-resolution microscopy techniques [17–20], the quantum state in NV center can be imaged and controlled at nanoscale. Therefore, the coupled NV centers promise an excellent experimental platform for the study of the photon-mediated dipole-dipole interaction process not only for quantum information techniques, but also for energy transfer investigations.

In the photon-mediated dipole-dipole interaction, the coupling strength is a key parameter for qubit manipulation in quantum information techniques and for transfer efficiency in energy transfer application. In principle, in order to enhance the coupling strength in the dipole-dipole interaction, the photon-atom interaction should be increased primarily. One of the effective methods to increase the photon-atom interaction is to couple the atom with surface plasmon polariton (SPP) on a metal surface [21–23] with high density of states and tight spatial confinement. Recently, researchers have demonstrated that SPP can assist energy transfer between two ensembles of fluorescent molecules on thin metal film and the enhancement factor of energy transfer efficiency can be 30 [5]. Also, coupling with SPPs on metal surface will enhance the interaction between two NV centers. Compared to metal nano-wires [22, 24], planar metal surface is easy to fabricate and has potential for scalable applications, based on that array of NV centers can be generated by ion implantation [14, 25, 26] near diamond surface with developing techniques [27–29].

In this paper, we focused on the negatively charged NV centers in diamond near various surfaces and systematically studied the coupling strength of coupled NV centers via their electric dipoles. In detail, the collective relaxation and coherent coupling of two NV centers near to air surface, metal surface and metal film are studied numerically with Green Function (GF) method. It is found that the coupling strength between two NV centers can be enhanced by the metal surface because of the SPPs. Also, the SPPs on both sides of the metal film can mediate the coupling of the two dipoles and thus further enhance the total coupling. The thickness of the metal film can provide a way to tune the coupling strength. Our investigation will present a systematical result for the photon-mediated atoms interaction on metal surface. It also provides detailed information for experimental applications based on coupling NV centers mediated with SPPs on metal film.

This paper is organized as follows. Section II describes the physical model of dipoles of NV centers, and the method we use to calculate the collective relaxation and coherent coupling of two dipoles. In Sec. III, we discuss two dipoles near to air surface. The coherent coupling and collective relaxation of two NV centers near to diamond and air interface are calculated. The lifetime of single dipole near to surface is also studied. In Sec. IV, we discuss two NV centers near to gold and silver surface, as in Sec. III. The enhancement of dipole-dipole coupling is studied. In Sec. V, two NV centers near to gold film are investigated and the cases of symmetrical and asymmetrical planar waveguide are both discussed. Finally, Sec. VI is the conclusion.

\* yap@ustc.edu.cn

† fwsun@ustc.edu.cn

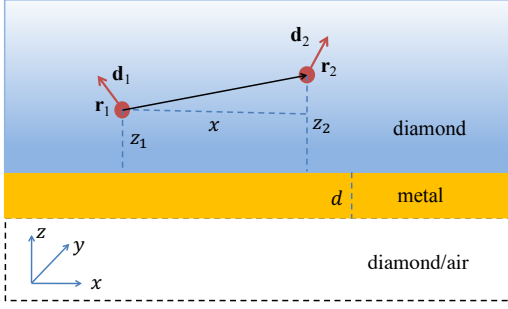


FIG. 1. Schematic of two dipoles (e.g., dipoles of NV centers) near metal surface. Two NV centers in diamond crystal near surface with electric dipoles  $\mathbf{d}_1$  and  $\mathbf{d}_2$  respectively are close to each other (denoted by NV1 and NV2). The thickness of the metal film is  $d$ . Under the metal film, it is air or diamond.

## II. PHYSICAL MODEL AND METHOD

Two NV centers close to each other in diamond crystal are considered here, as shown in Fig. 1. This is usually the case of implanted NV centers in experiment [14]. One of the two NV centers is assumed to be located at  $\mathbf{r}_1 = (0, 0, z_1)$  (denoted as NV1), and the other (denoted as NV2) is located at  $\mathbf{r}_2 = (x, 0, z_2)$  with a displacement  $\mathbf{r} = r(\sin \theta \cos \phi, \sin \theta \sin \phi, \cos \theta)$  with respect to NV1, where  $r$  is the distance between the two NV centers, and  $\theta$  and  $\phi$  are the polar angle and azimuthal angle of the displacement vector, respectively. For simplicity,  $\phi = 0$  is chosen here. NV center is a multi-level artificial atom and there are linearly polarization dipoles and circularly polarization dipoles with different directions [30]. The energy levels and allowed optical transitions of NV centers have been carefully discussed [30, 31].

Here, GF method from the electrodynamics is applied to study the coupling of NV centers. The collective relaxation and coherent coupling strength of two dipoles are described as [22, 24]:

$$\Gamma^{(12)} = \frac{\omega_A^2}{c^2 \hbar \epsilon_0} \text{Im}[\mathbf{d}_1 \cdot \overleftrightarrow{\mathbf{G}}(\mathbf{r}_1, \mathbf{r}_2, \omega_A) \cdot \mathbf{d}_2], \quad (1)$$

$$\Omega^{(12)} = \frac{1}{\pi \hbar \epsilon_0} \mathbf{P}_c \int_0^\infty \frac{\omega^2}{c^2} \frac{\text{Im}[\mathbf{d}_1 \cdot \overleftrightarrow{\mathbf{G}}(\mathbf{r}_1, \mathbf{r}_2, \omega_A) \cdot \mathbf{d}_2]}{\omega - \omega_A} d\omega, \quad (2)$$

where  $\overleftrightarrow{\mathbf{G}}(\mathbf{r}_1, \mathbf{r}_2, \omega_A)$  is the dyadic Green Function tensor of the electromagnetic field,  $\omega_A$  is the transition frequency of the dipole,  $c$  is the light velocity in vacuum and  $\mathbf{P}_c$  denotes the Cauchy value integral. It is noticed that we use  $\Gamma$  to denote the spontaneous damping rate of state amplitude, which adds a factor 1/2 compared to that of Ref. [24]. It is supposed that two dipoles  $\mathbf{d}_1$  and  $\mathbf{d}_2$  are with same transition frequency.

The Green function,  $\overleftrightarrow{\mathbf{G}}$ , gives a full description of the field and the coupling of dipoles. However, solving the full  $\overleftrightarrow{\mathbf{G}}$  for certain structure is usually difficult and numerical solution of the electromagnetic field equation is needed. Usually, the full

$\overleftrightarrow{\mathbf{G}}$  can be written as

$$\overleftrightarrow{\mathbf{G}} = \overleftrightarrow{\mathbf{G}}_0 + \overleftrightarrow{\mathbf{G}}_s, \quad (3)$$

where  $\overleftrightarrow{\mathbf{G}}_0$  is the free GF of dipole in isotropic homogenous medium and  $\overleftrightarrow{\mathbf{G}}_s$  is the scattering GF by the structure.

Single dipole couples with the electromagnetic field modes and decays from the excited state with spontaneous emission rate. When  $\mathbf{r}_1 = \mathbf{r}_2$ , the collective relaxation reduced to the spontaneous damping rate  $\Gamma = 1/(2\tau)$ , where  $\tau$  is the lifetime of dipole and can be measured by experiment. When the dipole is far away from the interface, the scattering GF can be eliminated and the spontaneous damping rate approaches

$$\Gamma_0 = \frac{\omega_A^2}{c^2 \hbar \epsilon_0} \text{Im}[\mathbf{d}_1 \cdot \overleftrightarrow{\mathbf{G}}_0(\mathbf{r}_1, \mathbf{r}_1, \omega_A) \cdot \mathbf{d}_1] = \frac{n\omega_A^3 d^2}{6\pi \epsilon_0 \hbar c^3}, \quad (4)$$

which is spontaneous damping coefficient in isotropic homogeneous medium. For dipoles of NV center in diamond,  $n = 2.418$  is the refractive index. The spontaneous emission lifetime is  $\tau_0 = 1/(2\Gamma_0) = 13.2$  ns typically.

Also, it is noticed that

$$\Gamma^{(12)} = \Gamma_0^{(12)} + \Gamma_s^{(12)}, \quad (5a)$$

$$\Omega^{(12)} = \Omega_0^{(12)} + \Omega_s^{(12)}, \quad (5b)$$

according to Eq. (3).  $\Gamma_s^{(12)}$  and  $\Omega_s^{(12)}$  with subscripts  $s$  denote the coupling and relaxation coefficients induced by the scattering GF. When  $r$  is not very small, the relaxation rate  $\Gamma_s^{(12)}$  and coherent coupling strength  $\Omega_s^{(12)}$  can always be written as [24]

$$\Gamma_s^{(12)} = \frac{\omega_A^2}{c^2 \hbar \epsilon_0} \text{Im}[\mathbf{d}_1 \cdot \overleftrightarrow{\mathbf{G}}_s(\mathbf{r}_1, \mathbf{r}_2, \omega_A) \cdot \mathbf{d}_2], \quad (6a)$$

$$\Omega_s^{(12)} = \frac{\omega_A^2}{c^2 \hbar \epsilon_0} \text{Re}[\mathbf{d}_1 \cdot \overleftrightarrow{\mathbf{G}}_s(\mathbf{r}_1, \mathbf{r}_2, \omega_A) \cdot \mathbf{d}_2]. \quad (6b)$$

Since the free GF  $\overleftrightarrow{\mathbf{G}}_0$  has an explicit expression (see Appendix VII A), the coherent coupling and collective relaxation contributed by  $\overleftrightarrow{\mathbf{G}}_0$  can be obtained easily, with similar expressions in Eq. (6a) and Eq. (6b). In the following, we will focus on the scattering GF in Eq. (6a) and Eq. (6b). There are several numerical methods to calculate the scattering GF of the system. For stratified medium, the method based on the Fresnel Law of electromagnetic field and the Wely Identity is an effective one [32, 33] (see Appendix VII B). It is noted that the theory here is valid for arbitrary depth and directions of dipoles, as the equations formulated in this work. For numerical calculation, we assume that two dipoles are with the same depth and consider only some typical cases in real experiment, where the two dipoles are parallel.

## III. NV CENTERS NEAR TO AIR SURFACE

NV centers in diamond are usually generated by ion implantation, with depth between several nanometers to tens of

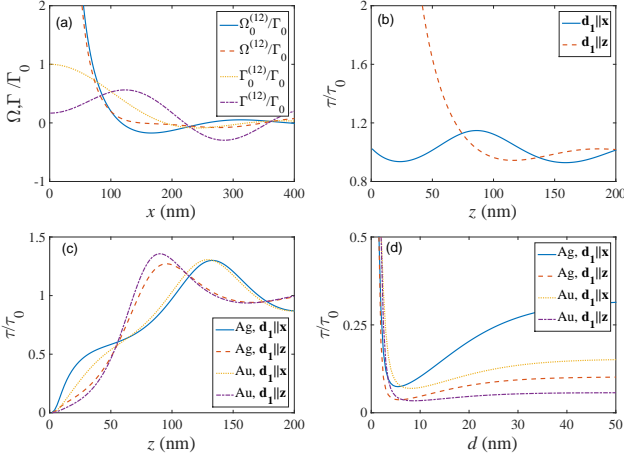


FIG. 2. (a) The coherent coupling  $\Omega_s^{(12)}$  and collective relaxation  $\Gamma_s^{(12)}$  for two NV center dipoles in diamond near to air surface, with different displacement along  $x$ . Two dipoles are both perpendicular to surface, e.g.,  $\mathbf{d}_1 \parallel \mathbf{z}$ ,  $\mathbf{d}_2 \parallel \mathbf{z}$ , and are both with depth 16 nm, e.g.,  $z_1 = z_2 = 16$  nm. (b) Lifetime of single NV center dipole  $\mathbf{d}_1$  in diamond near to air surface, with different depth  $z$ . Both the cases of  $\mathbf{d}_1 \parallel \mathbf{x}$  and  $\mathbf{d}_1 \parallel \mathbf{z}$  are shown. It is noted that the lifetime of the  $\mathbf{d}_1 \parallel \mathbf{z}$  dipole is not divergent but approaches 16.1 when distance  $z$  approaches 0. Similar phenomenon of lengthening the lifetime here can also be seen in Ref. [34]. (c) The lifetime of single dipole  $\mathbf{d}_1$  in diamond near to metal surface, with different depth  $z$ . Here, metal (gold or silver) has filled the semi-infinite space below the  $z = 0$  interface. (d) The lifetime of single dipole  $\mathbf{d}_1$  in diamond near to metal film surface, with different film thickness  $d$ . The dipoles are assumed to be located with depth 16 nm in diamond ( $z_1 = 16$  nm). In Fig.(c) and (d), both the cases of dipoles parallel ( $\mathbf{d}_1 \parallel \mathbf{x}$ ) and perpendicular ( $\mathbf{d}_1 \parallel \mathbf{z}$ ) to surface are shown.

nanometers. For example, under the 20 KeV energy ion-implantation, the depth of NV centers is distributed among 8 ~ 20 nm with a maximum at about 16 nm [14]. The coupling of two dipoles near to diamond and air interface is calculated in this section.

The two dipoles can have different directions. For simplicity, two dipoles both along  $z$  axis are considered first. The collective relaxation and coherent coupling coefficients induced by scattering GF can be expressed as

$$\begin{aligned} \Gamma_s^{(12)} &= \Gamma_0 \frac{6\pi}{k_1} \text{Im}[G_{s,zz}(\mathbf{r}_1, \mathbf{r}_2, \omega_A)] \\ &= \Gamma_0 \text{Re} \left[ \int_0^\infty d\xi J_0(k_1 x \xi) \frac{\xi^3 r^p e^{ik_1 \sqrt{1-\xi^2}(z_1+z_2)}}{\sqrt{1-\xi^2}} \right], \quad (7a) \end{aligned}$$

$$\begin{aligned} \Omega_s^{(12)} &= \Gamma_0 \frac{6\pi}{k_1} \text{Re}[G_{s,zz}(\mathbf{r}_1, \mathbf{r}_2, \omega_A)] \\ &= \Gamma_0 \text{Im} \left[ \int_0^\infty d\xi J_0(k_1 x \xi) \frac{\xi^3 r^p e^{ik_1 \sqrt{1-\xi^2}(z_1+z_2)}}{\sqrt{1-\xi^2}} \right]. \quad (7b) \end{aligned}$$

They are single variable integrals and can be calculated numerically. Among them,  $k_1$  is the wavevector in the diamond,  $x$  is the horizontal displacement as shown in Fig. 1,  $J_0$  is the

Bessel function,  $\xi$  is the integration variable.  $G_{s,zz}$  is the element of  $\vec{G}_s$ .  $r^s$  and  $r^p$  are the Fresnel reflection coefficients for  $s$  and  $p$  polarized light, respectively. Here, since both the two dipoles are along  $z$  axis,  $r^s$  doesn't appear (see Appendix VIII B).

The total coupling and relaxation coefficients according to Eq. (5a) and Eq. (5b) are calculated and shown in Fig. 2(a). We can see that, the collective relaxation coefficient near to surface is very different from that in diamond crystal. Due to the reflection of the free GF from the interface, the total GF changes considerably.

The relaxation rate ( $\Gamma$ ) of single NV center with dipole  $\mathbf{d}_1$  is also affected by surface and is discussed here. Normalized by  $\Gamma_0$ , it is

$$p = \frac{\Gamma}{\Gamma_0} = \frac{\text{Im}[\mathbf{d}_1 \cdot \vec{G} \cdot \mathbf{d}_1]}{\text{Im}[\mathbf{d}_1 \cdot \vec{G}_0 \cdot \mathbf{d}_1]} = 1 + \frac{6\pi}{k_1} \text{Im}[\hat{d}_{1,i} G_{s,ij} \hat{d}_{1,j}], \quad (8)$$

where  $\hat{d}_1$  is the normalized direction of dipole  $\mathbf{d}_1$  and  $i, j = x, y, z$  denote the Cartesian components of the dipole  $\mathbf{d}_1$ . When the dipole is perpendicular to the interface, i.e.,  $\mathbf{d}_1 \parallel \mathbf{z}$ , only  $i = z$  component is remained and  $p_\perp = 1 + \frac{6\pi}{k_1} \text{Im}[G_{s,zz}]$ , where  $p_\perp$  denotes the relaxation enhancement of dipole perpendicular to the surface. Similarly, the case of dipole parallel to the surface is computed as  $p_\parallel$ . Both  $p_\perp$  and  $p_\parallel$  are numerically calculated and shown in Fig. 2(b). Here, the GF reflected by the surface interferes with the free GF, so the relaxation rate (or the lifetime) oscillates with a period of half wavelength of the photons from NV center electric dipole.

For dipoles with angle  $\alpha$  with  $z$  axis, Eq. (8) is simplified as

$$p = 1 + \sin^2(\alpha) p_\parallel + \cos^2(\alpha) p_\perp. \quad (9)$$

There are dipoles of various directions in NV center ensemble, and the lifetime measurement in experiment gets the average lifetime of all kinds of dipoles.

#### IV. NV CENTERS NEAR TO METAL SURFACE

The metal with negative dielectric coefficient supports SPPs when  $\epsilon_{\text{metal}} < -\epsilon_{\text{dielectric}}$ . Dipoles near to metal surface can couple to SPPs and have large spontaneous damping rate. Two dipoles near metal surface can also have stronger coupling through the SPPs compared to that through the electromagnetic field in free space. Array of NV centers can be generated with well designed ion-implantation techniques and metal film can be deposited with controllable thickness. These techniques promise that array NV centers in diamond can be applied in the study of SPP enhanced electric dipole-dipole interaction for quantum information and energy transfer.

For the interface between dielectric material with dielectric constant  $\epsilon_1$  and metal material with dielectric constant  $\epsilon_2$ , the SPP modes have a wave vector

$$k_{sp} = k_0 \sqrt{\frac{\epsilon_1 \epsilon_2}{\epsilon_1 + \epsilon_2}} = k_1 \sqrt{\frac{\epsilon_2}{\epsilon_1 + \epsilon_2}}, \quad (10)$$

where  $k_0 = 2\pi/\lambda_0$  is vacuum wavevector,  $k_1 = 2\pi/\lambda_1$  is wave vector in dielectric material and  $\lambda_1 = \lambda_0/n$  is the wavelength in diamond here. For NV centers in diamond, the zero phonon line (ZPL) is  $\lambda_0 = 637.2$  nm. The dielectric coefficient of Au is  $\varepsilon_2 = -10.85 + 1.27i$  at this wavelength [35]. The imaginary part of the dielectric coefficient results in both phase change and absorption.  $\varepsilon_1 = 5.847$  is the dielectric coefficient of diamond. So, in this system the SPP mode has a wavelength  $\lambda_{sp} = 181.5$  nm.

The coherent coupling and collective relaxation of two dipoles on metal surface are shown in Fig. 3. The case of both dipoles perpendicular to the surface, i.e.,  $\mathbf{d}_1 \parallel \mathbf{z}, \mathbf{d}_2 \parallel \mathbf{z}$ , is shown in Fig. 3(a), while Fig. 3(b) is for  $\mathbf{d}_1 \parallel \mathbf{x}, \mathbf{d}_2 \parallel \mathbf{x}$ . Here, we consider only the scattering GF induced coupling. In principle, the free space coupling should be added to get the total coupling. However, it can be neglected when the dipoles are near to surface and the distance between two dipoles are not very small. We can see that the coupling is much stronger than that in free space or on dielectric surface. Since the SPP modes have approximate analytic solutions [36, 37], the approximated expression of relaxation and coupling can also be expressed as

$$\frac{\Gamma_s^{(12)}}{\Gamma_0} = \frac{6\pi}{k_1} \text{Re}[G_{xx}(\mathbf{r}_1, \mathbf{r}_2, \omega_A)] \quad (11)$$

$$\approx c_1 \text{Im}[c_2 e^{i(k_{sp}x + k_{sp}^z(z_1 + z_2) - \frac{\pi}{4})} / \sqrt{k_{sp}x}], \quad (12)$$

$$\frac{\Omega_s^{(12)}}{\Gamma_0} = \frac{6\pi}{k_1} \text{Im}[G_{xx}(\mathbf{r}_1, \mathbf{r}_2, \omega_A)] \quad (13)$$

$$\approx c_1 \text{Re}[c_2 e^{i(k_{sp}x + k_{sp}^z(z_1 + z_2) - \frac{\pi}{4})} / \sqrt{k_{sp}x}]. \quad (14)$$

The approximation results of Eq. (12) and Eq. (14) are also plotted in Fig. 3(a)(b) for two dipoles both with 20 nm depth, where  $c_1$  and  $c_2$  are complex coefficients independent of  $x$ . We can see that it is indeed a good approximation when the dipole depth is much smaller than the wavelength.

The coupling coefficient will increase when the two dipoles approach the metal surface. As we can see in Fig. 3(b)(c), the coupling becomes stronger when the distance  $z$  decreases. The oscillating period of coupling coefficient is the surface plasmon wavelength  $\lambda_{sp}$ . The line for infinite distance is the total coupling coefficient of two dipoles in dielectric material. The case for the silver surface is also studied. The coupling and relaxation of both dipoles parallel and perpendicular to surface are plotted in Fig. 3(e)(f). The dielectric constant of silver is  $\varepsilon_{Ag} = -14.69 + 1.21i$  [35] at the wavelength of the ZPL of NV center.

The lifetime of a dipole near to metal surface is shown in Fig. 2(c). When the distance away from the metal surface is at the scale of wavelength, the lifetime of a dipole is modulated by the interference. At this time, the dipoles mainly emit free photons mostly. It is similar to the case of dielectric material. When the dipole is approaching the metal with distance much less than  $\lambda_1/2$ , it couples to the SPP modes and the lifetime decreases very much. When distance  $z$  is very small, there is dipole emission quenching. The dielectric coefficient model of metal used here will be invalid, and thus the lifetime of

dipole can not approach to 0 when  $z \rightarrow 0$ .

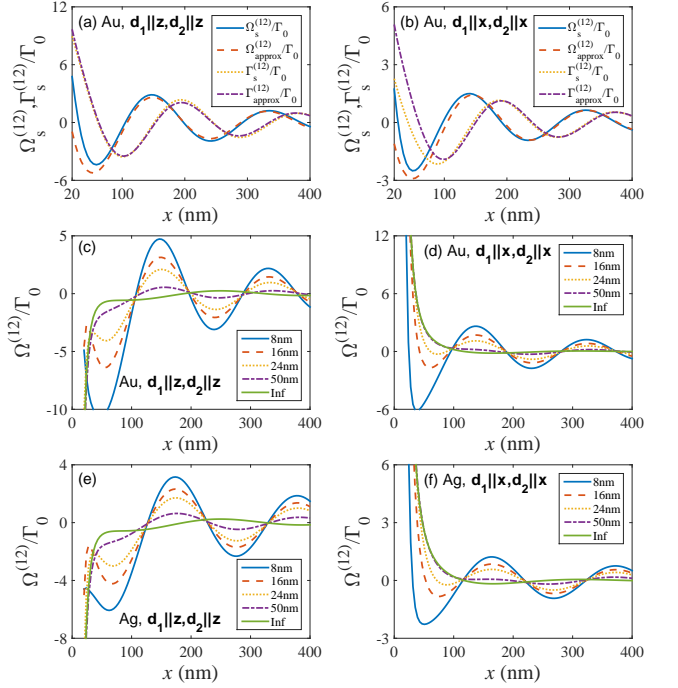


FIG. 3. (a)(b) The coherent coupling coefficient  $\Omega_s^{(12)}$  and collective relaxation  $\Gamma_s^{(12)}$  for two dipoles in diamond on Au surface, with different displacement along  $x$ . Two dipoles are both located with depth 20 nm in diamond ( $z_1 = z_2 = 20$  nm). The  $y$  direction displacement of two dipoles is 0. Theoretic approximations are shown for comparison. (a) is for two dipoles both perpendicular to surface,  $\mathbf{d}_1 \parallel \mathbf{z}, \mathbf{d}_2 \parallel \mathbf{z}$ . (b) is for two dipoles both parallel to surface,  $\mathbf{d}_1 \parallel \mathbf{x}, \mathbf{d}_2 \parallel \mathbf{x}$ . (c)(d)(e)(f) The coupling coefficient  $\Omega_s^{(12)}$  for two dipoles in diamond on gold and silver surface, with different displacement along  $x$ . Two dipoles both with depth 8 nm, 16 nm, 24 nm and 50 nm are shown. The depth *Inf* is for two dipoles far away from surface, i.e., in homogeneous diamond material. (c) is for two dipoles both perpendicular to gold surface,  $\mathbf{d}_1 \parallel \mathbf{z}, \mathbf{d}_2 \parallel \mathbf{z}$ . (d) is for gold surface,  $\mathbf{d}_1 \parallel \mathbf{x}, \mathbf{d}_2 \parallel \mathbf{x}$ . (e) is for silver surface,  $\mathbf{d}_1 \parallel \mathbf{z}, \mathbf{d}_2 \parallel \mathbf{z}$ . (f) is for silver surface,  $\mathbf{d}_1 \parallel \mathbf{x}, \mathbf{d}_2 \parallel \mathbf{x}$ .

## V. NV CENTERS NEAR TO METAL FILM

When the metal material is a film with thickness much less than wavelength, the SPP modes on both sides of the film can affect the dipole-dipole interaction and the lifetime of a single dipole. The lifetime of NV center dipoles on metal film surface (downside of the film is air) is shown in Fig. 2(d). When the thickness of film  $d > 50$  nm, the lifetime of a dipole stays the same as that on metal surface. For the case of a dipole perpendicular ( $\mathbf{d}_1 \parallel \mathbf{z}$ ) to gold surface, when  $10 \text{ nm} < d < 50 \text{ nm}$ , the SPP modes on the downside of the film can couple to the dipole and reduce the lifetime. The lifetime is decreased to a minimum when  $d \approx 10$  nm. When the thickness  $d < 10$  nm, the bounding of light to SPP modes becomes weaker, and the lifetime increases. Lifetime of dipoles parallel to gold film surface and lifetime of dipoles on silver film surface are also shown. For these cases, the lifetime reduces to minimum at a



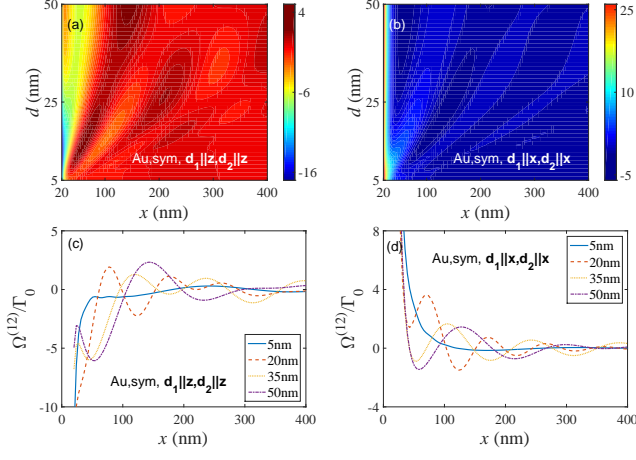


FIG. 4. The coupling coefficient  $\Omega^{(12)}$  for two dipoles in diamond on symmetrical gold film surface, with different displacement along  $x$  and different film thickness  $d$ . (a) Two dipoles are both perpendicular to surface, i.e.,  $\mathbf{d}_1 \parallel \mathbf{z}, \mathbf{d}_2 \parallel \mathbf{z}$ . (b) Two dipoles are both parallel to surface, i.e.,  $\mathbf{d}_1 \parallel \mathbf{x}, \mathbf{d}_2 \parallel \mathbf{x}$ . (c)(d) Line cuttings of (a) and (b), respectively. The gold film with thickness  $d = 5$  nm, 20 nm, 35 nm and 50 nm are shown. In these figures, two dipoles are both located at the depth 16 nm in diamond ( $z_1 = z_2 = 16$  nm).

smaller thickness (about 5 nm), and other behaviors keep the same.

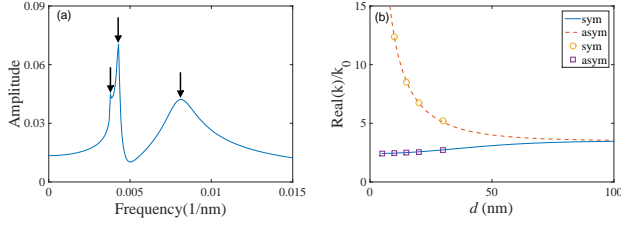


FIG. 5. The modes mediated in the dipole-dipole interaction and the dispersion relation of the symmetrical and asymmetrical modes of symmetric gold planar waveguide. (a) Fourier transform of the coupling coefficient  $\Omega^{(12)}$  for two dipoles both with depth 30 nm to surface and direction perpendicular to surface, i.e.,  $\mathbf{d}_1 \parallel \mathbf{z}, \mathbf{d}_2 \parallel \mathbf{z}$ . (b) The effective refractive indices of SPP modes supported by the gold film with different thickness  $d$ . The lines are the numerical solutions of the dispersion equation for SPP modes. The symbols are for the modes from (a), with film thickness  $d = 5$  nm, 10 nm, 15 nm, 20 nm and 30 nm, respectively.

The film thickness dependence of dipole-dipole interaction near to symmetrical metal film is shown in Fig. 4(a)(b). And Fig. 4(c)(d) are some line cuttings of Fig. 4(a)(b) with certain thicknesses. It can be seen that, with the decrease of the film thickness, the frequency of the SPP increases.

For symmetrical metal film with same dielectric constant on both sides, the coupling between two dipoles is induced by free electromagnetic field modes in diamond, symmetrical SPP mode and asymmetrical SPP mode of the metal film. To show this, the Fourier transform of the coupling strength on the symmetrical metal film with thickness 30 nm is shown

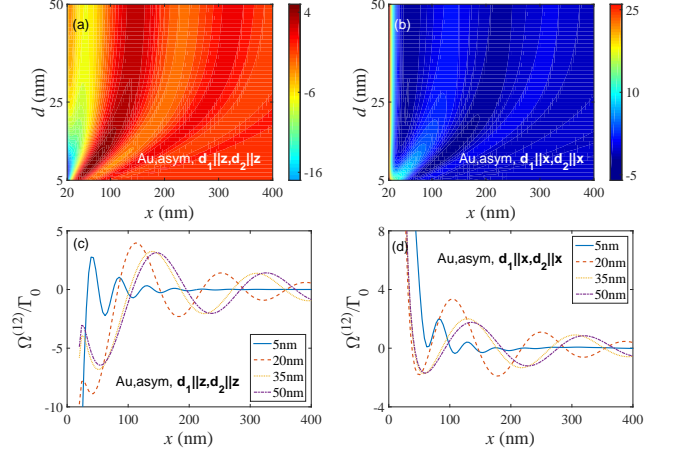


FIG. 6. The coupling coefficient  $\Omega^{(12)}$  for two dipoles in diamond on asymmetrical gold film surface, with different displacement along  $x$  and different film thickness  $d$ . The substrate is changed from diamond to air compared to Fig. 4. Other parameters are the same as Fig. 4.

in Fig. 5(a). The three maxima corresponds to three modes at spatial frequency 0.0038/nm, 0.0043/nm, and 0.0081/nm, with effective refractive indices 2.426, 2.745, and 5.170, respectively. It is analyzed that they are free mode, symmetrical mode and asymmetrical mode respectively. The cases for film thickness with  $d = 5$  nm, 10 nm, 15 nm, 20 nm and 30 nm are also calculated. The symmetrical and asymmetrical modes are shown in Fig. 5(b). The solid and dashed lines in Fig. 5(b) are the numerical solutions of the dispersion equation of symmetrical metal film for SPP modes [38]. It can be seen that they match very well and verifies our analysis.

The coherent coupling coefficient of two dipoles on asymmetrical metal planar waveguide is also studied. The result is shown in Fig. 6. Here, the material below the gold film is changed from diamond to air, as in Fig. 1. The phenomenon of coupling on asymmetrical waveguide is similar with that on symmetrical waveguide.

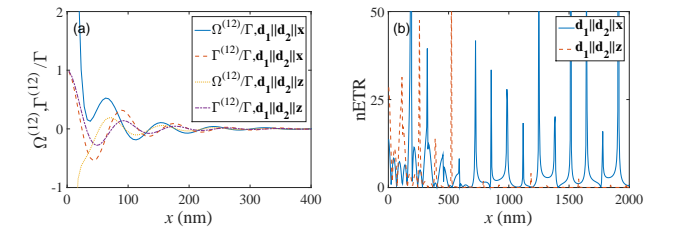


FIG. 7. (a)  $\Omega^{(12)}$  and  $\Gamma^{12}$  normalized by  $\Gamma$  for two dipoles in diamond on asymmetrical gold film surface, with different displacement along  $x$ . The film thickness  $d = 10$  nm. (b) The normalized energy transfer rate for two dipoles with directions  $\mathbf{d}_1 \parallel \mathbf{d}_2 \parallel \mathbf{z}$  and  $\mathbf{d}_1 \parallel \mathbf{d}_2 \parallel \mathbf{x}$ .

Fig. 7 shows the enhancement of coherent coupling and the energy transfer for the two dipoles in diamond on asymmetrical gold film surface. The  $\Omega^{(12)}$  and  $\Gamma^{12}$  normalized by  $\Gamma$  is shown in Fig. 7(a). Here, we choose the total decay rate  $\Gamma$  of

the dipole near the metal film as the normalizing constant, so we can see at which displacement that the coupling exceeds the decay rate. It can be seen that  $\Omega^{(12)}/\Gamma$  surpasses 1 only for distance less than 25 nm, which means that both the coupling and relaxation are enhanced by SPPs.

The normalized energy transfer rate (nETR) between two dipoles are defined as [39]

$$nETR = \Gamma^{(12)}/\Gamma_0^{(12)}, \quad (15)$$

where  $\Gamma^{(12)}$  is the collective relaxation in the presence of the metal film and  $\Gamma_0^{(12)}$  is the collective relaxation in isotropic homogeneous medium (i.e., diamond here). The results are shown in Fig. 7(b). It's noted that the dipole directions of NV centers are fixed, which is different from fluorescent molecules. For two fluorescent molecules, the acceptor dipole is induced by the field from the donor dipole [33, 39]. The nETR should be averaged over various dipole directions [5]. Thus the nETR defined here for two NV center dipoles is a little different. Here, the two dipoles are with determined direction and the nETR has sharp points when  $\Gamma_0^{(12)} = 0$ . The energy transfer rate has been increased by tens of times for both  $\mathbf{d}_1\|\mathbf{d}_2\|\mathbf{z}$  and  $\mathbf{d}_1\|\mathbf{d}_2\|\mathbf{x}$  for most of distances between the dipoles. Also, nETR for  $\mathbf{d}_1\|\mathbf{d}_2\|\mathbf{x}$  keeps large with distance of 2  $\mu\text{m}$  and is larger than that for  $\mathbf{d}_1\|\mathbf{d}_2\|\mathbf{z}$ . This distance is the same as the distance between array of NV centers generated by current techniques of ion implantation [25, 26].

## VI. DISCUSSION AND CONCLUSION

In conclusion, we have investigated the enhanced electric dipole-dipole interaction near to various surfaces, especially near to the metal planar film. Starting from the general theory of GF method for stratified media, the collective relaxation and coherent coupling of two dipoles of NV centers near to dielectric surface, metal surface and metal film are calculated. The results verify the enhanced electric-dipole coupling by SPPs on metal surface and provide a systematical result for experimental applications. Also, it is found that the waveguide thickness changes the coupling coefficients of two dipoles, through changing of the efficiency and ratio of the coupling of dipole emissions to different modes of waveguide. It thus provides a method to tune the coupling of two dipoles. Such a SPP enhanced dipole-dipole interaction in NV center system would be a promising experimental platform for the study of quantum information techniques and energy transfer.

**Acknowledgments.** This work is supported by Strategic Priority Research Program (B) of the Chinese Academy of Sciences (Grant No. XDB01030200), the National Natural Science Foundation of China (Grant Nos. 11374032, 11374290, 91536219, 61522508), Anhui Provincial Natural Science Foundation (Grant Nos. 1508085SMA205, 1408085MKL0), and the Fundamental Research Funds for the Central Universities.

## VII. SUPPLEMENTAL MATERIAL

The appendices have been written for the readability, as a concise introduction of the method used in this work. Details can be seen in related references [32, 33, 40].

### A. Dyadic Green Function tensor

The dyadic GF  $\overleftrightarrow{G}_0$  of isotropic homogenous medium for dipole emission is the solution of

$$\nabla \times \nabla \times \overleftrightarrow{G}_0(\mathbf{r}_1, \mathbf{r}_2, k) - k^2 \overleftrightarrow{G}_0(\mathbf{r}_1, \mathbf{r}_2, k) = I\delta(\mathbf{r}_1, \mathbf{r}_2), \quad (16)$$

and can be explicitly expressed as

$$\overleftrightarrow{G}_0(\mathbf{r}_1, \mathbf{r}_2, k) = [I + \frac{1}{k^2} \nabla \nabla] \frac{e^{ikr}}{4\pi r} \quad (17a)$$

$$= \frac{e^{ikr}}{4\pi r} [(1 - \frac{1}{ikr} - \frac{1}{(kr)^2})I + (-1 + \frac{3}{ikr} + \frac{3}{(kr)^2})\hat{r}\hat{r}] + \frac{\delta(r)}{3k^2}I \quad (17b)$$

$$= \frac{ke^{ikr}}{4\pi} [(\frac{1}{kr} + \frac{i}{(kr)^2} - \frac{1}{(kr)^3})I - (\frac{1}{kr} + \frac{3i}{(kr)^2} - \frac{3}{(kr)^3})\hat{r}\hat{r}] + \frac{\delta(r)}{3k^2}I. \quad (17c)$$

In these equations,  $k$  is the wave vector in the medium,  $I$  is the three-order unit tensor,  $r = |\mathbf{r}_2 - \mathbf{r}_1|$  and  $\hat{r} = \overrightarrow{\mathbf{r}}/r$  is the unit vector. We denote the three-order tensor  $\overleftrightarrow{G}_0$  with row and column indices  $x, y, z$ .

### B. Green Function of stratified medium

Weyl Identity [33] states that

$$\frac{e^{ikr}}{r} = \frac{i}{2\pi} \int \int \frac{e^{i(k_x x + k_y y + k_z |z|)}}{k_z} dk_x dk_y. \quad (18)$$

Using this identity we can decompose the free GF as planar wave with different angular spectrum. Each planar wave is reflected by the interface and all the reflected waves constitute the scattering GF. At the same time, the scattering GF on the other side of the interface is constituted by transmitted waves. The reflection and transmission coefficients are described by Fresnel Law. Explicitly, the scattering GF by reflection is

$$\overleftrightarrow{G}_s(\mathbf{r}, \mathbf{r}_0) = \frac{i}{8\pi^2} \int \int_{-\infty}^{\infty} (\overleftrightarrow{M}_s^s + \overleftrightarrow{M}_s^p) * e^{i[k_x(x-x_0) + k_y(y-y_0) + k_{1z}(z+z_1)]} dk_x dk_y, \quad (19)$$

where

$$\overleftrightarrow{M}_s^s = \frac{r^s(k_x, k_y)}{k_{1z}(k_x^2 + k_y^2)} \begin{bmatrix} k_y^2 & -k_x k_y & 0 \\ -k_x k_y & k_x^2 & 0 \\ 0 & 0 & 0 \end{bmatrix}, \quad (20a)$$

$$\overleftrightarrow{M}_s^p = \frac{-r^p(k_x, k_y)}{k_1^2(k_x^2 + k_y^2)} * \begin{bmatrix} k_x^2 k_{1z} & k_x k_y k_{1z} & k_x(k_x^2 + k_y^2) \\ k_x k_y k_{1z} & k_y^2 k_{1z} & k_y(k_x^2 + k_y^2) \\ -k_x(k_x^2 + k_y^2) & -k_y(k_x^2 + k_y^2) & -\frac{(k_x^2 + k_y^2)^2}{k_{1z}} \end{bmatrix}. \quad (20b)$$

In these equations,  $r^s$  and  $r^p$  are Fresnel reflection coefficients and  $k_{1z}$  is the  $z$  component of wave vector in the incident medium (denoted as medium 1). Fresnel Law can be written

in the wave vector form:

$$r^s(k_x, k_y) = \frac{\mu_2 k_{1z} - \mu_1 k_{2z}}{\mu_2 k_{1z} + \mu_1 k_{2z}}, \quad (21a)$$

$$r^p(k_x, k_y) = \frac{\varepsilon_2 k_{1z} - \varepsilon_1 k_{2z}}{\varepsilon_2 k_{1z} + \varepsilon_1 k_{2z}}, \quad (21b)$$

$$t^s(k_x, k_y) = \frac{2\mu_2 k_{1z}}{\mu_2 k_{1z} + \mu_1 k_{2z}}, \quad (21c)$$

$$t^p(k_x, k_y) = \frac{2\varepsilon_2 k_{1z}}{\varepsilon_2 k_{1z} + \varepsilon_1 k_{2z}} \sqrt{\frac{\mu_2 \varepsilon_1}{\mu_1 \varepsilon_2}}. \quad (21d)$$

Fresnel Law of this form is valid for various kinds of wave vectors, including those in cases of total reflection and metal reflection. For single layer medium as we discuss here, Fresnel Law can be expressed as

$$r = \frac{r_{12} + r_{23} e^{2ik_2 d}}{1 + r_{12} r_{23} e^{2ik_2 d}}, \quad (22a)$$

$$t = \frac{t_{12} t_{23} e^{ik_2 d}}{1 + r_{12} r_{23} e^{2ik_2 d}}, \quad (22b)$$

for  $s$  and  $p$  wave respectively, where  $r_{12}$ ,  $r_{23}$ ,  $t_{12}$ ,  $t_{23}$  are Fresnel coefficients on respective layer interfaces and  $d$  is the thickness of the film. For multi-layer medium, Fresnel coefficients have a similar form which can be got with recursion [40].

- 
- [1] R. Dicke, Coherence in spontaneous radiation processes, *Phys. Rev.* **93**, 99 (1954).
- [2] M. Gross and S. Haroche, Superradiance: An essay on the theory of collective spontaneous emission, *Phys. Rep.* **93**, 301 (1982).
- [3] M. Scheibner, T. Schmidt, L. Worschech, A. Forchel, G. Bacher, T. Passow, and D. Hommel, Superradiance of quantum dots, *Nature Phys.* **3**, 106 (2007).
- [4] H. Bernien, B. Hensen, W. Pfaff, G. Koolstra, M. Blok, L. Robledo, T. Taminiau, M. Markham, D. Twitchen, L. Childress, and R. Hanson, Heralded entanglement between solid-state qubits separated by three metres, *Nature* **497**, 86 (2013).
- [5] D. Bouchet, D. Cao, R. Carminati, Y. De Wilde, and V. Krachmalnicoff, Long-range plasmon-assisted energy transfer between fluorescent emitters, *Phys. Rev. Lett.* **116**, 037401 (2016).
- [6] P. Andrew and W. L. Barnes, Energy transfer across a metal film mediated by surface plasmon polaritons, *Science* **306**, 1002 (2004).
- [7] H. T. Dung, L. Knöll, and D.-G. Welsch, Intermolecular energy transfer in the presence of dispersing and absorbing media, *Phys. Rev. A* **65**, 043813 (2002).
- [8] C. A. Marocico and J. Knoester, Effect of surface-plasmon polaritons on spontaneous emission and intermolecular energy-transfer rates in multilayered geometries, *Phys. Rev. A* **84**, 053824 (2011).
- [9] S. Yang, D. Z. Xu, Z. Song, and C. P. Sun, Dimerization-assisted energy transport in light-harvesting complexes, *J. Chem. Phys.* **132**, 234501 (2010).
- [10] A. C. Benniston and A. Harriman, Artificial photosynthesis, *Mater. Today* **11**, 26 (2008).
- [11] M. R. Wasielewski, Photoinduced electron transfer in supramolecular systems for artificial photosynthesis, *Chem. Rev.* **92**, 435 (1992).
- [12] A. Siphahigil, K. D. Jahnke, L. J. Rogers, T. Teraji, J. Isoya, A. S. Zibrov, F. Jelezko, and M. D. Lukin, Indistinguishable photons from separated silicon-vacancy centers in diamond, *Phys. Rev. Lett.* **113**, 113602 (2014).
- [13] A. Gruber, A. Dräbenstedt, C. Tietz, L. Fleury, J. Wrachtrup, and C. v. Borczyskowski, Scanning confocal optical microscopy and magnetic resonance on single defect centers, *Science* **276**, 2012 (1997).
- [14] T. Yamamoto, C. Müller, L. McGuinness, T. Teraji, B. Naydenov, S. Onoda, T. Ohshima, J. Wrachtrup, F. Jelezko, and J. Isoya, Strongly coupled diamond spin qubits by molecular nitrogen implantation, *Phys. Rev. B* **88**, 201201 (2013).
- [15] F. Jelezko and J. Wrachtrup, Single defect centres in diamond: A review, *Phys. Stat. Sol. (a)* **203**, 3207 (2006).
- [16] M. W. Doherty, N. B. Manson, P. Delaney, F. Jelezko, J. Wrachtrup, and L. C. Hollenberg, The nitrogen-vacancy colour centre in diamond, *Phys. Rep.* **528**, 1 (2013).
- [17] E. Rittweger, K. Y. Han, S. E. Irvine, C. Eggeling, and S. W. Hell, Sted microscopy reveals crystal colour centres with nanometric resolution, *Nature Photon.* **3**, 144 (2009).
- [18] J.-M. Cui, F.-W. Sun, X.-D. Chen, Z.-J. Gong, and G.-C. Guo, Quantum statistical imaging of particles without restriction of the diffraction limit, *Phys. Rev. Lett.* **110**, 153901 (2013).
- [19] X. Chen, C. Zou, Z. Gong, C. Dong, G. Guo, and F. Sun, Subdiffraction optical manipulation of the charge state of nitrogen vacancy center in diamond, *Light: Sci. Appl.* **4**, e230 (2015).
- [20] M. Pfender, N. Aslam, G. Waldherr, P. Neumann, and J. Wrachtrup, Single-spin stochastic optical reconstruction mi-

- croscopy, *Proc. Natl. Acad. Sci.* **111**, 14669 (2014).
- [21] G. W. Ford and W. Weber, Electromagnetic interactions of molecules with metal surfaces, *Phys. Rep.* **113**, 195 (1984).
- [22] A. Gonzalez-Tudela, D. Martin-Cano, E. Moreno, L. Martin-Moreno, C. Tejedor, and F. J. Garcia-Vidal, Entanglement of two qubits mediated by one-dimensional plasmonic waveguides, *Phys. Rev. Lett.* **106**, 020501 (2011).
- [23] F. Zhou, Y. Liu, and Z.-Y. Li, Surface-plasmon-polariton-assisted dipole-dipole interaction near metal surfaces, *Opt. Lett.* **36**, 1969 (2011).
- [24] D. Dzsotjan, J. Kästel, and M. Fleischhauer, Dipole-dipole shift of quantum emitters coupled to surface plasmons of a nanowire, *Phys. Rev. B* **84**, 075419 (2011).
- [25] J. Meijer, B. Burchard, M. Domhan, C. Wittmann, T. Gaebel, I. Popa, F. Jelezko, and J. Wrachtrup, Generation of single color centers by focused nitrogen implantation, *Appl. Phys. Lett.* **87**, 261909 (2005).
- [26] J. Wang, F. Feng, J. Zhang, J. Chen, Z. Zheng, L. Guo, W. Zhang, X. Song, G. Guo, L. Fan, C. Zou, L. Lou, W. Zhu, and G. Wang, High-sensitivity temperature sensing using an implanted single nitrogen-vacancy center array in diamond, *Phys. Rev. B* **91**, 155404 (2015).
- [27] K. Ohno, F. Joseph Heremans, L. C. Bassett, B. A. Myers, D. M. Toyli, A. C. Bleszynski Jayich, C. J. Palmstrom, and D. D. Awschalom, Engineering shallow spins in diamond with nitrogen delta-doping, *Appl. Phys. Lett.* **101**, 082413 (2012).
- [28] J. Wang, W. Zhang, J. Zhang, J. You, Y. Li, G. Guo, F. Feng, X. Song, L. Lou, W. Zhu, and G. Wang, Coherence times of precise depth controlled nv centers in diamond, *Nanoscale* **8**, 5780 (2016).
- [29] C. A. McLellan, B. A. Myers, S. Kraemer, K. Ohno, D. D. Awschalom, and A. C. B. Jayich, Patterned formation of highly coherent nitrogen-vacancy centers using a focused electron irradiation technique, *Nano Lett.* **16**, 2450 (2016).
- [30] J. R. Maze, A. Gali, E. Togan, Y. Chu, A. Trifonov, E. Kaxiras, and M. D. Lukin, Properties of nitrogen-vacancy centers in diamond: the group theoretic approach, *New J. Phys.* **13**, 025025 (2011).
- [31] N. B. Manson, J. P. Harrison, and M. J. Sellars, Nitrogen-vacancy center in diamond: Model of the electronic structure and associated dynamics, *Phys. Rev. B* **74**, 104303 (2006).
- [32] M. Paulus, P. Gay-Balmaz, and O. J. F. Martin, Accurate and efficient computation of the green's tensor for stratified media, *Phys. Rev. E* **62**, 5797 (2000).
- [33] L. Novotny and B. Hecht, *Principles of nano-optics* (Cambridge university press, 2012).
- [34] R. Ruppin and O. J. F. Martin, Lifetime of an emitting dipole near various types of interfaces including magnetic and negative refractive materials, *J. Chem. Phys.* **121**, 11358 (2004).
- [35] M. N. Polyanskiy, *Refractive index database* (Online; accessed 2-June-2016).
- [36] F. J. García de Abajo, Colloquium: Light scattering by particle and hole arrays, *Rev. Mod. Phys.* **79**, 1267 (2007).
- [37] N. Rotenberg, M. Spasenović, T. L. Krijger, B. le Feber, F. J. García de Abajo, and L. Kuipers, Plasmon scattering from single subwavelength holes, *Phys. Rev. Lett.* **108**, 127402 (2012).
- [38] J. J. Burke, G. I. Stegeman, and T. Tamir, Surface-polariton-like waves guided by thin, lossy metal films, *Phys. Rev. B* **33**, 5186 (1986).
- [39] D. Martín-Cano, L. Martín-Moreno, F. J. García-Vidal, and E. Moreno, Resonance energy transfer and superradiance mediated by plasmonic nanowaveguides, *Nano Lett.* **10**, 3129 (2010).
- [40] W. C. Chew, *Waves and fields in inhomogeneous media*, Vol. 522 (IEEE press New York, 1995).